Protective films on complex substrates of thermoplastic and cellular elastomers

Martínez-Martínez, D.; Tiss, B.; Glanzmann, L. N.; Wolthuizen, D. J.; Cunha, L.; Mansilla, C.; De Hosson, J. Th M.

Published in:
Surface and Coatings Technology

DOI:
10.1016/j.surfcoat.2022.128405

Surface & Coatings Technology 442 (2022) 128405

Contents lists available at ScienceDirect

Surface & Coatings Technology

journal homepage: www.elsevier.com/locate/surfcoat

Protective films on complex substrates of thermoplastic and cellular elastomers: Prospective applications to rubber, nylon and cork

D. Martínez-Martínez [a,c,d,*], B. Tiss [a], L.N. Glanzmann [b], D.J. Wolthuizen [d], L. Cunha [a], C. Mansilla [b], J.Th.M. De Hosson [d,**]

[a] Center of Physics of the University of Minho and Porto, Campus de Azurem, 4800-058 Guimaraes, Portugal
[b] CTECHnano Coatings Technologies S.L., Tolosa Hiribidea 76, 20018 San Sebastián, Spain
[c] Department of Materials Research and Technology, Luxembourg Institute of Science and Technology (LIST), 28 avenue des Hauts-Fourneaux, Esch-sur-Alzette L-4362, Luxembourg
[d] Department of Applied Physics, Zernike Institute for Advanced Materials, University of Groningen, Nijenborgh 4, 9747AG Groningen, the Netherlands

ARTICLE INFO

Keywords:
Thermoplastic elastomers
Cellular elastomers
Cork
Rubber
Nylon
Wear
Friction
UV light
Discoloration

ABSTRACT

Deposition of thin films is an appropriate methodology to enhance the performance of a material by modification of its surface, while keeping the properties of the bulk largely unaffected. However, a practical implementation becomes less straightforward when dealing with sensitive or complex substrates, for instance, those which cannot be subjected to harsh treatments, such as cleaning and etching, or extreme deposition conditions, like high temperatures, and ion impingement et cetera.

This paper concentrates on deposition processing of complex substrates. In particular, it discusses the deposition of two types of protective coatings (diamond-like carbon (DLC) films against friction and wear, and TiO_2 films against UV light) on three types of thermoplastic and cellular elastomers (rubber, nylon and cork). It is demonstrated that a successful protection of thermoplastic elastomers against wear with DLC films can be attained, after a thorough adaptation of the procedure to the characteristics of the specific substrate. In addition, the paper reports the very first depositions on a cellular elastomer like cork by vapor deposition methods, including Atomic Layer Deposition (ALD).

1. Introduction

Surface engineering holds a rather unique place in engineering history, since the surface of a component is usually the predominant engineering factor. An important reason is that the surface of a work-piece is often subjected to wear and corrosion in practical use. In industrialized countries, a substantial portion of all energy generated is ultimately lost through friction [1,2], which should also become a major concern when putting topics of 'energy transition' and 'climate change' on the political agenda [3]. As a consequence, the search for suitable surface engineering techniques has been activated in the past decades resulting in an almost bewildering choice of surface treatments that cover a wide range of thickness [4]. As a general rule of thumb, the choice has to be such that the surface treatment does not impair too much the properties of the substrate for which it was originally chosen. For instance, it should not reduce the load bearing capabilities of the substrate, e.g. the capacity of absorbing mechanical energy of cellular materials like cork.

Obviously, all the levels of the morphological complexity at different length scales of the substrate are issues of major concern as regard the deposition methodology applied. Actually, intrinsic aspects of the substrate have been overlooked quite frequently in surface engineering, with emphasis exclusively on the materials properties of the protective coating itself. Here it is worthy to note that tribo-properties are not materials properties but embrace also extrinsic properties determined not only by the intrinsic materials properties as such but also by the complete system [5].

For a long time, the hardness (H) has been regarded as a primary material property affecting wear resistance. However, the elastic strain to failure, which is related to the H/E ratio, is a more suitable parameter for predicting wear resistance [6], where E represents the Young's

* Correspondence to: D. Martínez-Martínez, Department of Materials Research and Technology, Luxembourg Institute of Science and Technology (LIST), 28 avenue des Hauts-Fourneaux, Esch-sur-Alzette L-4362, Luxembourg.
** Corresponding author.
E-mail addresses: diegus.m2@gmail.com (D. Martínez-Martínez), j.t.m.de.hosson@rug.nl (J.Th.M. De Hosson).

https://doi.org/10.1016/j.surfcoat.2022.128405

Available online 26 March 2022

modulus. Within a linear-elastic approach, this is understandable according to the relations which show that the yield stress of contact is proportional to (H^3/E^2) [7,8]. In addition, the equation for the fracture toughness reads $G_c = \pi a {\sigma_c}^2/E$, with a the crack length and σ_c the critical stress at failure [9]. This indicates that the fracture toughness of coatings, defined by the so-called 'critical strain-energy release rate' G_c, would be improved by both a low E modulus and a high hardness H. These aspects of the interplay of two opposing properties, like ductility and hardness, have been emphasized in the work by Adrian Leyland and Allan Matthews [10,11]. Increasing hardness also means an increase in the elasticity strain limit and a reduction in ductility, leading to a lowering of fatigue resistance and hence to brittle failure. The characteristics of the system, i.e. whether the wear is caused by delamination or abrasion [5], determine which of the surface engineering methods should be chosen.

Equally, the surface treatment chosen should be suitably related to the problem to be solved. Physical and chemical vapor deposition techniques, including Atomic Layer Deposition (ALD), are most commonly employed in order to obtain controlled films with tailored properties [12]. As afore-mentioned, not surprisingly, the traditional focus lies on coating on top of rigid substrates, e.g. deposition of ductile metallic (inter)layers on hard substrates [13]. However, these findings are not easily transferable to flexible (thermoplastic) elastomers substrates like rubber, due to the non-metallic character of the substrate and the requirement of maintaining flexibility of the complete system of a substrate and a coating on top. In addition, elastomers may exhibit a much higher roughness and classical polishing is not possible, in contrast for instance to rigid substrates. We reviewed several strategies for a successful deposition of highly adherent protective coatings on elastomers and rubbers [14], where we have stressed various differences with traditional approaches that are explored on rigid substrates (e.g. steel or silicon).

In this paper, results are presented showing that successful depositions on sensitive and/or flexible substrates entails some new opportunities, but also exciting new challenges with respect to complicated substrate morphology. This statement is particularly true for protective applications, since in that case the film must show an excellent adhesion to the substrate in order to accomplish its functionality. Specifically, the processing steps and conditions of thermoplastic elastomers and cellular elastomers are discussed. In particular, we confine ourselves to three cases (rubber, nylon and cork), and two environments to protect against (friction and UV exposure), with DLC and TiO_2 films, respectively.

2. Experimental details

Diamond-like carbon (DLC) films were deposited on ACM rubber (alkyl acrylate copolymer) and nylon pieces (Nylon 6–6 extruded, thickness 1.6 mm, Professional Plastics) by means of bias-induced Plasma Assisted Chemical Vapor Deposition (PACVD) in a Teer UDP/400 close field unbalanced magnetron sputtering rig (ca. 30 L volume), with all the magnetrons powered off. A pulsed DC (p-DC) power unit (Advanced Energy) was used as substrate bias source, operating at 250 kHz with a pulse off time of 500 ns (duty cycle 87.5%). The nominal voltages were varied between 300 V and 600 V, which represent a minimum value to obtain a reasonable deposition rate and stable plasma conditions, and a value close to the maximum achievable by the power unit, respectively. The substrates were clamped at one corner over metallic plates and mounted on the substrate carrousel rotating at 3 rpm to ensure film homogeneity. The deposition process was composed of three steps. At the first one, the substrates were etched for 30–40 min in an Ar plasma (15 sccm, 5×10^{-3} mbar) to clean further the surface from contaminations. Then, a second treatment in a plasma mixture of Ar and H_2 (flow ratio 15:10 sccm, 6×10^{-3} mbar) was used to improve the adhesion of the forthcoming carbonaceous layer. In the final step, H_2 is replaced by C_2H_2 (10 sccm) and a DLC film is deposited.

TiO_2 coatings were deposited by magnetron sputtering in a modified EVA chamber (Aliance Concept) on cork (Amorim Cork Composites) and rubber-resin composites (FlowCo) substrates hanging in a rotating holder (5.5 rpm) placed at 70 mm from the magnetron head. The base pressure during depositions was 5.4×10^{-6} mbar. The depositions were performed by sputtering of a Ti target (99.6% at., $100 \times 200 \times 6$ mm^3) using Ar (25 sccm) and O_2 (5.5 sccm) as working and reactive gases, respectively, resulting in a working pressure of 4.1×10^{-3} mbar. The power source was operated in dc mode, current controlled at 2.0 A, with a registered target voltage of 422 ± 3 V. The substrates were not intentionally heated during film deposition.

ALD depositions were carried out in a Coating Technologies S.L. (CTECHnano) Fluidized Bed Reactor (FBR), equipped with a TARNOS vibration table to assist fluidization of the particles loaded in a vertical 250 mm stainless steel reactor column of 25 mm inner diameter. Titanium tetrachloride ($TiCl_4$, Sigma Aldrich/Merck) and demineralized water were used as metal precursor and oxidizing agent, respectively. The N_2 gas flows during precursor dosing and purging were 200 and 400 sccm, respectively. The process temperature was set to 120 °C. 1 g of cork grains (Amorim Cork Composites) were processed with a dose-purge-dose-purge sequence of 90s-300s-90s-300s for $TiCl_4$ and water to deposit 200 cycles of titania (TiO_2). The X-ray reflectivity (X'pert PRO by PANalytical) of the control Si wafer placed in the reactor outlet during the processes resulted in thin film thicknesses of 20 nm titania.

The microstructure of the samples was characterized by scanning electron microscopy using a Philips FEG-XL30s operating at 3 kV, and a FEI Quanta 400 FEG ESEM operating at 10 kV. Cross sections of DLC film coated on rubber were obtained by fracture after immersion in liquid nitrogen for 10 min.

The roughness of surfaces was evaluated with a Nanofocus® confocal microscope, using NanoFocus μSurf v.6.1 software for analysis. An MTS Nanoindenter XP® was employed to measure the hardness (H) and modulus (E) of substrates with a Berkovich indenter.

The tribological performance was evaluated at room temperature on a CSM tribometer with a ball-on-disk configuration, operating at room temperature in air at 35 ± 2% relative humidity controlled by a humidity regulator. The counterpart was a ∅6 mm commercial 100Cr6 steel ball (60–62 HRC, Ra < 32 nm). The tests were carried out in unlubricated conditions with 1 N normal load, 20 cm/s sliding speed unless otherwise specified, and 10,000 laps length. For reference, the tribological properties of a Delrin plate (Acetal Homopolymer, Delrin 14% AF, thickness 3.2 mm, Professional Plastics) were also evaluated.

Optical spectrophotometry was performed with a commercial Minolta CM-2600d portable spectrophotometer (wavelength range: 360–700 nm) to quantify the color of the samples according to CIELab 1976 L*a*b* color space [15] in the three color coordinates. L* indicates the color lightness, and it varies from zero (black) to 100 (white). a* and b* are the chromaticity coordinates, where the transition from positive to negative values indicate color variations from green to red, and blue to yellow, respectively. The diffuse and specular components of reflection of light were measured, without the UV 400 nm cut filter, and with a 3 mm aperture mask. The variation of color (ΔC) between a sample and a reference (subindex R) can be measured with the following equation:

$$\Delta C = \sqrt{\left(L^* - L_R^*\right)^2 + \left(a^* - a_R^*\right)^2 + \left(b^* - b_R^*\right)^2} \quad (1)$$

3. Results and discussion

As a starting point of our research of the deposition of thin films on complex substrates, the tribological performance of elastomers with DLC coated films is taken as a reference. The essence of the methodology and representative results on rubber will be summarized first in Section 3.1, followed by the results obtained for more complex substrates, such as rigid polymers and cork, in Sections 3.2 and 3.3.

3.1. DLC films on elastomers for anti-wear and anti-friction protection

Among polymers, elastomers are probably the most difficult to work with when adding protective layers on top. In addition to temperature sensitivity, they show resilience and viscoelasticity, which forces the deposited coating to be flexible and adherent. However, as aforementioned, traditional solutions used to coat rigid substrates are not applicable due to the non-metallic character of the substrate and the requirement of maintaining flexibility of the complete material system. Another issue is that an elastomer like rubber shows a high roughness and polishing is not possible. Moreover, in many cases the presence of filler particles increases the complexity of the situation, since they may create adhesion problems in particular sites on the surface. Finally, rubbers are typically 'dirty' substrates to operate with. For instance, waxes like stearamide are known to be added to improve the processability of the rubber, which can migrate to the surface during ageing after the deposition of a coating [16,17]. Sometimes, even other residues can be found, due to manufacturing and production processing. Therefore, proper cleaning is mandatory to achieve good adhesion. However, chemicals have to be used with care, since polymers may be modified when using organic solvents (for instance, the typically used acetone or ethanol).

Table 1 summarizes the details for cleaning and deposition of DLC coatings on rubber specimens, which can be described by 5 sequential steps. It is worth mentioning that 4 of these 5 steps are devoted to set-up the rubber before the actual deposition takes place, in order to ensure a good adhesion of the coating. Before deposition, the rubber substrates were cleaned by two subsequent washing and boiling procedures, with the intention of removing dirt, grease, and any other contamination from the as-received material, and to remove any of the paraffin wax (melting temperature of 55–65 °C), respectively. Therefore, the first treatment is comprised of five cycles of ultrasonic washing in a 10 vol% solution of detergent (Superdecontamine 33 from N.V. Intersciences S. A., Brussels) in demineralized water at 60 °C for 15 min per cycle. The second one corresponds to five cycles of ultrasonic washing in boiling demineralized water for 15 min each cycle. Once washing is finished, rubber pieces are transferred to the deposition chamber, where they are clamped. Reaching good vacuum conditions may take long due to the porous nature of the substrate, but 6–8 h are typically enough to reach a good base pressure below 10^{-5} mbar. The next steps are subsequent plasma etching under Ar and Ar/H_2 mixtures; the former contributes to eliminate any possible residue that may be still present on the surface, while the presence of hydrogen in the latter promotes the surface activation for the subsequent deposition process. After this step, hydrogen is progressively replaced by the organic precursor in the deposition chamber (C_2H_2 in our case) and the deposition of the DLC is carried out.

To promote the flexibility of the DLC film, it was decided to use the high thermal expansion coefficient of rubber to our advantage. Thus, deposition voltages during plasma etching and deposition were selected to create large temperature variations during the growth of the film [18]. To fine tune those processes and quantify the temperature variation during film growth, the temperature was measured during plasma exposure at different bias voltages (300, 400, 500 and 600 V) by inserting a thermocouple in the rubber. Next, the temperature-time curves obtained were fitted assuming that the plasma is acting as a 'hot body', whose temperature (T_{eq}) depends only on the voltage, and creates a heat transfer (Q) to the rubber according to Fourier's law:

$$\frac{\partial Q}{\partial t} = -\lambda A \frac{\partial T}{\partial z} \tag{2}$$

where A is the substrate area, λ is the thermal conductivity and z represents the distance to the substrate. The temperature variation (ΔT) for a certain heat transfer depends on the specific heat capacity (c) and mass of the substrate (m), according to:

$$\Delta T = \frac{Q}{c \bullet m} \tag{3}$$

Eqs. (2) and (3) can be combined, and the resulting differential equation can be solved to reach the following equation:

$$ln\left(\frac{T - T_{eq}}{T_0 - T_{eq}}\right) = -K \bullet t \tag{4}$$

where T_0 is the temperature at the onset of the plasma treatment, and K is a constant that depends on the material properties of the rubber and the configuration of the system. Fittings of the abovementioned temperature-time curves to Eq. (4) allowed us to obtain T_{eq} for each plasma voltage and the value of K, which is a constant that depends on the type of rubber, but not on the voltage applied [5,7,9].

With these parameters, it is possible to define etching-deposition protocols to fine control the temperature variation during film growth, and to predict its value. In total, three of these deposition protocols are depicted in Fig. 1. Fig. 1a shows a deposition protocol where the temperature is kept constant during the growth of the film (constant voltage of 400 V during deposition and most of etching). As illustrated in the schematics, the dimensions of the substrate remain constant during the whole deposition, and a conventional columnar growth is observed. As a result, the film is continuous without the presence of cracks. In contrast, Fig. 1b illustrates an example of a film growing during a temperature rise of ΔT = 101 °C, since the voltage during plasma etching (300 V) is lower than during deposition (600 V). Therefore, the film grows on an expanding substrate, and a continuous film cannot be formed in the beginning of the film growth, as schematically shown. A continuous film can be formed only when the rate of expansion decreases. Additional rubber expansion leads to nucleation of cracks, which are subsequently closed inwards when the film is cooled down to room temperature. This film is therefore cracked, with an average patch size of 124 μm. Finally, the third example shows the opposite situation, where the plasma etching is carried out at a higher voltage (600 V) than the deposition (300 V). Consequently, the variation of temperature during growth is negative, ΔT = −94 °C, which leads to a shrinkage of the substrate during the whole deposition of the film. In this case, the film experiences a compressive stress right from the very beginning of the deposition, which leads to the earlier formation of cracks in comparison to the previous case, as well as a much denser network of cracks (patch size 39 μm). This explains why the patch size is smaller for negative temperature variations with similar values of |ΔT|; a positive temperature variation leads to the appearance of tensile stresses during film growth, which delays the formation of cracks in comparison with compressive stresses [18].

It is worth mentioning that, in both cases, the cracks are closed inwards, since films are subjected to compressive stress after cooling down to room temperature. In contrast to other approaches [10], this method avoids the exposure of the substrate to the environment at any time. The adhesion of these films were tested with the method designed by Allan Mathews and collaborators [19], which consists of stretching the substrate and evaluating the behavior of the DLC film. The response of the films was the formation of new cracks instead of detachments from the substrate, which indicates a superb adhesion of the films [8].

The deposition of any of these DLC films causes a marked decrease of

Table 1
Cleaning and deposition protocol used for the deposition of adherent DLC coatings on rubber.

Step	Condition	Repetitions and length
Washing	Detergent solution (10% vol.), 60 °C, ultrasounds	5 × 15 min
	Distilled water, 100 °C, ultrasounds	5 × 15 min
Plasma treatment	Ar, 300–600 V, pulsed dc	1 × 30–35 min
	Ar/H_2, 300–600 V, pulsed dc	1 × 10 min
Deposition	Ar, C_2H_2, 300–600 V, pulsed dc	1 × 45–120 min

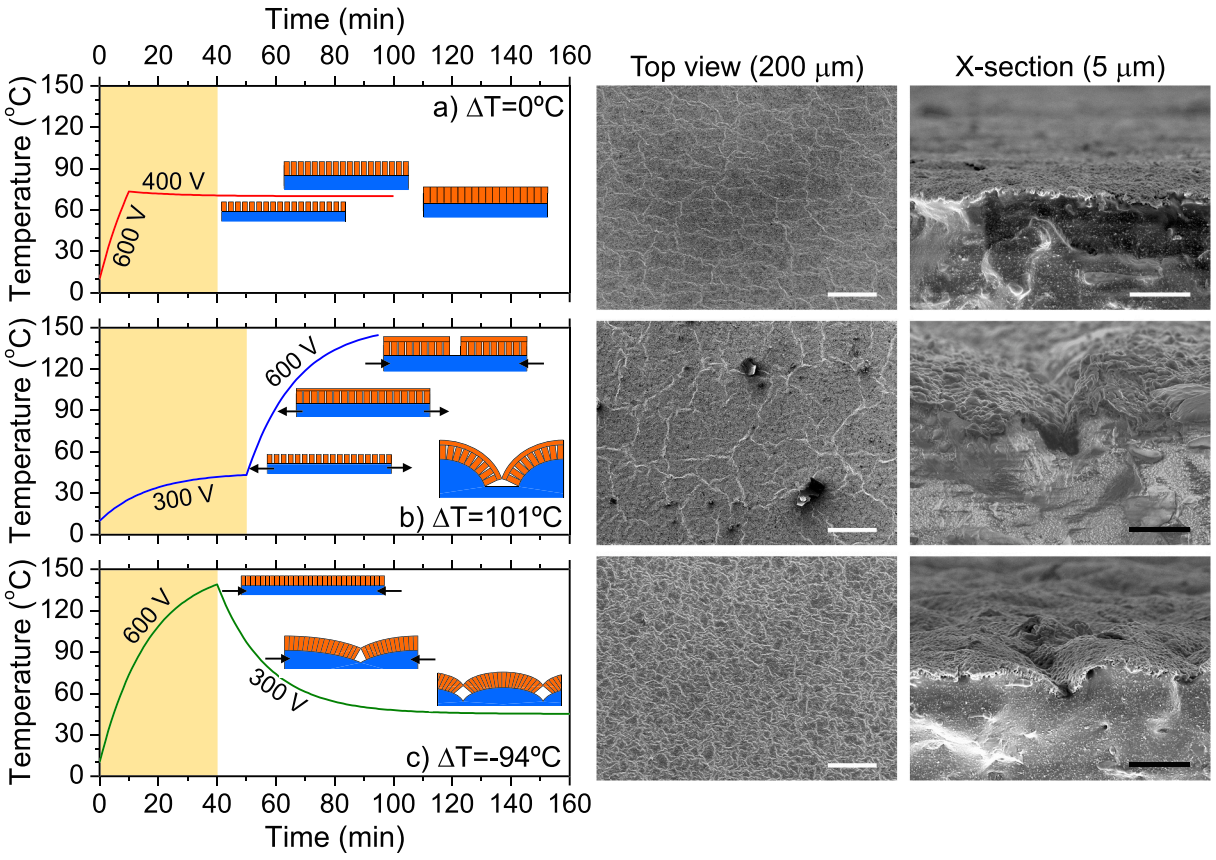

Fig. 1. Temperature-time curves representing three deposition protocols employed to obtain films with different microstructure. Labels indicate the voltages employed. Plasma etching previous deposition (i.e. without C_2H_2) is highlighted with a yellow background. a) Constant temperature during deposition (ΔT = 0). b) Heating during deposition (ΔT = 101 °C). c) Cooling during deposition (ΔT = -94 °C). Schematics representing different stages during growth of the films are included in each case. Top view and cross section SEM images of the three films after the deposition are included on the right part of the plot (scale bars: 200 μm and 5 μm, respectively).

the coefficient of friction (CoF) in comparison with the uncoated rubber substrate, as it is shown in Fig. 2. The enhanced tribological performance is also observed on the wear rate of the specimens, since negligible differences can be appreciated between SEM images acquired before and after tribotest. In contrast, the wear track is perfectly clear in the uncoated rubber [5]. The shape of the CoF curves of the coated samples is remarkable, since none of them attains a steady state. This behavior is depends on the type of rubber [16,20], and it is caused by the viscoelastic characteristics of the rubber substrate, leading to a variable size and shape of the contact area between the counterpart ball and the film [14,20–23]. It can be also observed that the increase of sliding speed of the tribotest from 5 to 20 cm/s leads to increased values of CoF for the three coated samples. In addition, among the three DLC films, the one without cracks (grown at ΔT = 0, red and pink curves) shows the highest value of CoF for all the testing speeds. Lower values of CoF are observed for the film with a patch size of 124 μm (deposited at ΔT = 101 °C, blue curves). Finally, the film with the patch size of 39 μm (prepared at ΔT = 101 °C, green curves) exhibit the lowest CoFs for the three testing speeds. It appears that a smaller patch size leads to a better frictional behavior [18,20], which is attributed to a higher flexibility of the deposited film-substrate system [14].

Although knowledge has been obtained of the correlations between synthesis conditions, microstructure, and performance of the films, detailed models providing quantitative insights are still lacking behind, e.g. only a qualitative model is designed that explains the different microstructure of the DLC films depending on the temperature variation experienced by the rubber substrate (Fig. 1). However, the design of a dynamic model of crack formation in DLC coated rubber during deposition is still pending. Such a model should offer a quantitative correlation between crack density (or patch size) and deposition characteristics, provided that the deposition conditions and the properties of the rubber are known. In that regard, 'in situ' optical measurements of cracks formation during film growth would be of great help. Another topic for in-depth future analysis concerns the phenomenological correlation between low friction and high crack density. In fact, a quantitative model description does not exist explaining why better flexibility will lead to a lower friction.

3.2. *DLC films on nylon for anti-wear and anti-friction protection*

After the successful deposition of DLC films on rubber, our objective is aimed at transferring the knowledge obtained to rigid substrates of similar chemical nature. Therefore, the goal was to deposit a DLC film on a conventional cheap thermoplastic elastomer of nylon, in order to obtain a performance similar to the one of Delrin. Previously, other authors have made different attempts to deposit DLC films on similar substrates. Niemczyk et al. [24] prepared H-free DLC films by pulsed laser deposition in polyamide 12 lab-made thin foils (130 μm). Nuclear magnetic resonance revealed that the 'bulk' substrate was not modified after the DLC deposition. However, they observed an intermixing layer between the DLC film (thickness < 80 nm) and substrate, which was supposed to provide a good adhesion, although it was not confirmed experimentally (e.g. scratch or frictional tests). The hardness of the film deposited on Si was ca. 20 GPa; on polyamide, the deposition of the DLC film increased clearly the hardness of the substrate (0.3 GPa), but it was not possible to measure accurately. Igarashi et al. [25] deposited a-C:H

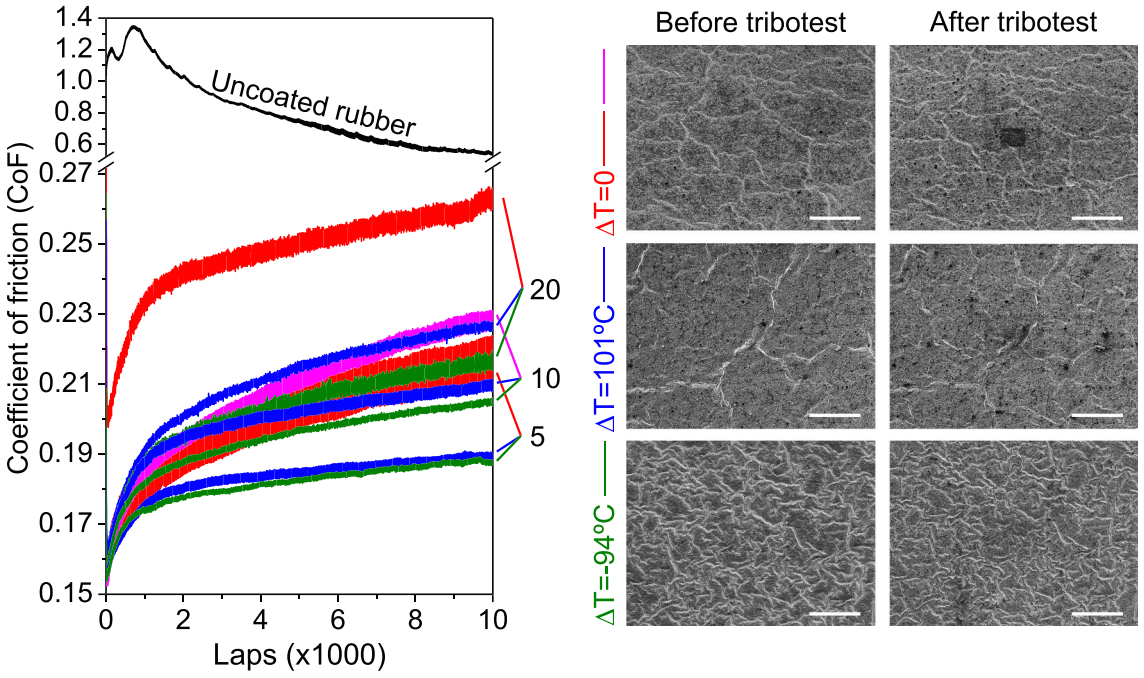

Fig. 2. Coefficient of friction (CoF) of DLC films deposited on rubber at different temperature variations during growth: ΔT = 0 (continuous film), ΔT = 101 (patch size 124 μm), and ΔT = -94 °C (patch size 39 μm). Each film was subjected to tribotests performed at three different test velocities (5, 10 and 20 cm/s), indicated with labels. The CoF of uncoated rubber (black line) is also included for comparison. SEM images (scale bars: 100 μm) acquired on coated substrates before and after the tribotests performed at 10 cm/s are included on the right part of the figure (same areas of the respective top-view images in Fig. 1).

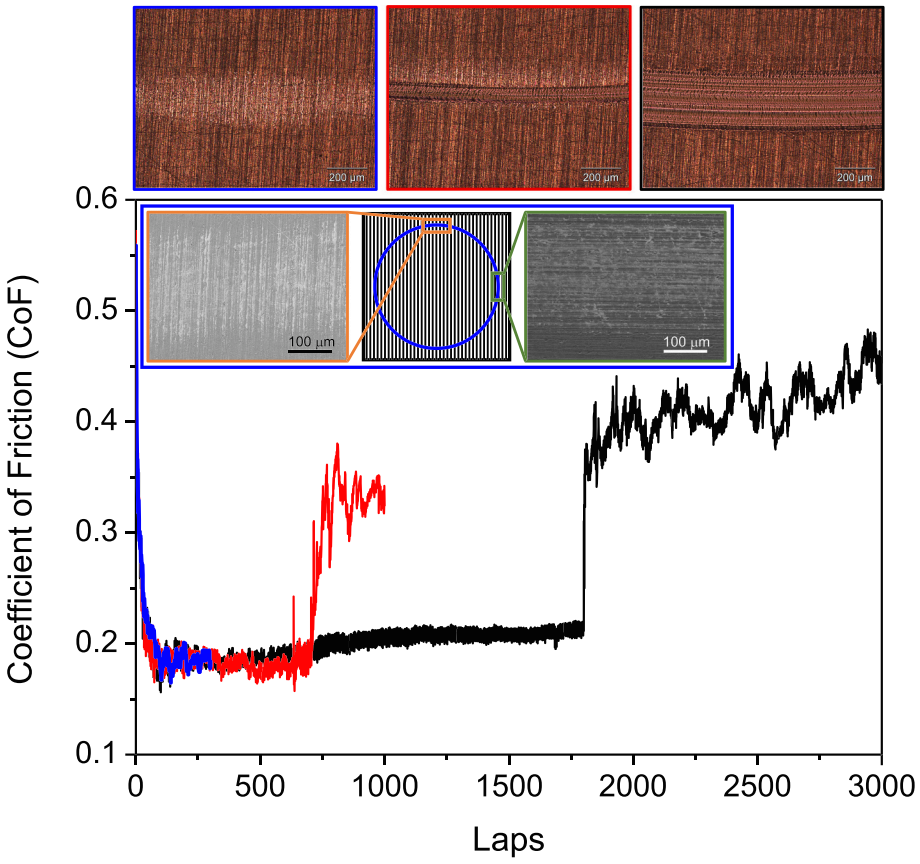

Fig. 3. Coefficient of friction of a DLC film deposited on unpolished nylon stopped at different test length: before failure (blue curve), immediately after failure (red curve) and after the whole test (black curve, only represented 3000 laps of 10,000). In the top, optical images of the wear track after these three tests. SEM images included as insets illustrate two regions of the film before failure with processing lines of the nylon parallel and perpendicular to the direction of the wear track, respectively, as indicated in the scheme.

films on lab-made injection-molded into disks (5 mm) of a polymer alloy consisting of nylon 66 matrix and modified poly(phenylene ether) by plasma-based ion implantation and deposition. To obtain good adhesion, the deposition comprised four steps: Ar/CH_4 etching, Si implantation and two involving DLC deposition with C_2H_2 and toluene precursors. The film had a thickness of 1 μm, and it showed an adhesive strength >2.4 MPa, and a clear improvement of hardness (from ca. 0.12 to 3 GPa). Fruth et al. [26] used magnetron sputter ion plating from a graphite target to deposit a-C and DLC films on a commercial polyamide (A3HG5, BASF). They kept the deposition temperature < 150 °C to avoid substrate degradation.

To optimize the adhesion, they used 3 cleaning steps (alcohol, water, drying at 60 °C), and explored 3 different etching pre-treatments (Ar, O_2 and Ar + O_2) and 3 types of underlayer (Ti, Cr, Al). The best conditions showed and adhesion strength of ca. 15 MPa, and the mechanical properties were clearly improved (the Young's modulus increased from 6.8 to 45–50 GPa). The tribological behavior showed a clear improvement from the uncoated substrate, with friction coefficients of ca. 0.25 and 0.12 for a-C and DLC films, respectively (on relatively short tests of 5 s). Baba and Ratada [27] deposited DLC films on Nylon with plasma source ion implantation using pulsed-dc biasing. The deposition of the DLC film was carried out with C_2H_2, and the three different pre-treatment plasmas (H_2O, O_2 and CH_4) lead to similar adhesion ca. 300–400 kg/cm^2. The frictional curve was smooth and in the range of 0.2–0.25 for 2000 cycles, almost half of the noisier curve of the uncoated substrate (CoF of 0.5).

In our case, we first followed the same procedure as described for elastomers in the previous section. However, it was found soon that such an approach was not appropriate, due to the machining lines on the commercial nylon substrates. Fig. 3 shows the tribological behavior of a DLC film deposited on nylon. During the first laps (<500), the CoF was more or less stable at 0.2. However, at some point it was observed that the CoF suffered a sudden increase to values, nearly doubled, which was indicative of the failure of the film. To study that process in detail, images were taken of the wear track of tribo-tests stopped at different times: before failure (blue curve in Fig. 3), immediately after failure (red curve) and the whole test (10,000 laps, black curve in Fig. 3). The image after the whole test reveals a large damage of the substrate, with a whole penetration on it. In contrast, in the test performed before failure, only scratches on the top of the grooves can be observed. SEM images acquired at different points of the wear track (regions parallel and transverse to the machining lines of the substrate, respectively, cf. scheme in Fig. 3) show that, indeed, wear is correlated to these machining lines, i.e., the film fails first in regions located in the top of these grooves. Finally, the image acquired immediately after the failure (red curve) displays a situation intermediate to the previous ones; the scratches on the top of the grooves can be still distinguished, but a severe damaging (of a similar kind as observed at the end of the test) can be detected in the center of the wear track.

As a consequence of these results, polishing was employed to remove these machining lines. However, that treatment revealed a complex structure of the nylon pieces, and different types of finishing could be attained depending on the polishing. These possibilities are summarized in Fig. 4. A relatively strong polishing (sandpaper P 500) removes the relatively 'hard' external layer of the substrate (H ~ 0.12 GPa, and reduced modulus E^* ~ 3.17 GPa) to reach a 'soft' inner core of the substrate (H ~ 0.014 GPa, E^* ~ 0.46 GPa), i.e., values one order of magnitude lower. Such a difference may be attributed to the processing of nylon sheets. Severe polishing reaches a finishing which is still rough (R_a ~ 150 nm), although not anisotropic, since the machining lines are removed (the roughness parallel to the machining lines is R_a ~ 80 nm). A gentle polishing (sandpaper P 2400 or higher) is able to reduce the roughness of both surfaces (hard or smooth) to R_a ~ 70 nm, and it allows to get rid of the machining lines without entering the soft region.

Finally, in addition to these four possibilities (hard or soft, rough or smooth), it was observed that the nylon substrates submerged into boiling water showed some curvature, indicating a difference of properties through the thickness of the nylon substrates. As a result, both sides of the nylon sheets did not show the same properties after polishing; the convex side showed a much lower coefficient of friction (0.07) than the concave side (0.35–0.45).

The frictional behavior of the best DLC film deposited on nylon after several tests is shown in Fig. 5, in comparison with the untreated as-received nylon and Delrin. Such DLC film was deposited on the convex side after rough-soft finishing, avoiding any cleaning procedure or plasma etching before deposition; other combinations failed. The DLC film lasts the entire test (10,000 laps) with a stable CoF around 0.22, which is much better than the CoF of untreated nylon (noisier CoF around 0.44). These values are in line with previous results [26,27]. The wear rate has also clearly improved from 2.1 ± 0.1 × 10^{-4} to 8.0 ± 1.0 × 10^{-6} mm^3/(N·m), the latter being equivalent to the wear rate observed for Delrin. Finally, it is worth mentioning that to reach a well-performing film, it was important to avoid any disturbance of the soft region (i.e., through cleaning and/or plasma etching). Also, rough finishing is preferred over the smooth finishing, probably because of an improved anchorage of the DLC film to the nylon substrate.

Sharing the lessons learned: an apparently simple substrate such as commercial nylon revealed an unexpected complex structure (8 possible types of finishing, considering roughness, polishing depth, and side), which constitutes a major challenge to tune all the parameters and processes to deposit an adherent protective layer. The complexity of this tuning process is in line with literature, where different approaches need to be followed to achieve adherent DLC films on substrates of close chemistry to Nylon [24–27]. To find out the reasons behind the

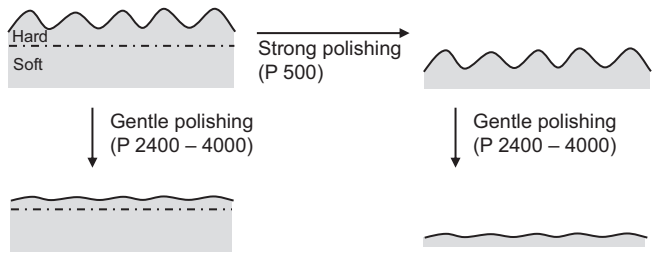

Fig. 4. Scheme of the inner structure of the nylon found after polishing, with a hard layer on the outside (where the processing lines are located) and a soft interior. The possible finishing status that can be reached depending on the polishing sequence are also illustrated. See main text for details.

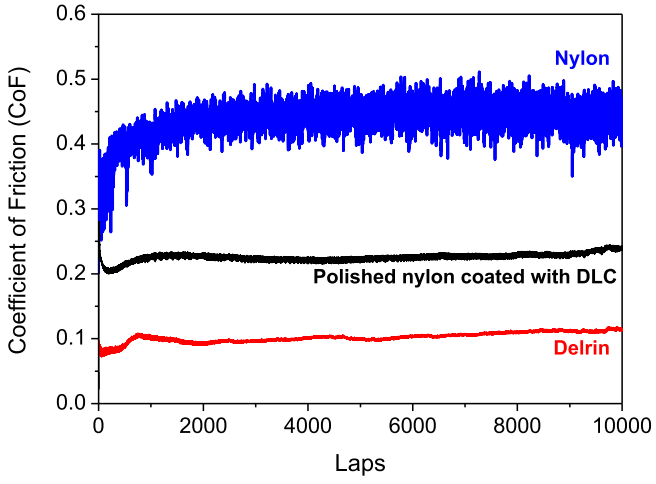

Fig. 5. Coefficient of friction of a polished nylon substrate successfully coated with a DLC film. Curves of uncoated as-received nylon and Delrin tested in the same conditions are included for reference.

appropriate finishing-adhesion relationship, future work should focus on the chemical nature of the different sub-layers found on nylon sheets. Future analyses should also be able to explain the reasons of the apparent high sensitivity of the nylon surface, since inappropriate cleaning or pre-deposition treatments lead to DLC films with rather poor adhesion.

3.3. TiO_2 films on cork and rubber for UV-protection

Ultraviolet radiation of sunlight is responsible for almost all discoloration of material products. This is also the case of cork, which is a natural material extracted from the external layer of the *Quercus suber* (the cork oak), and it shows many interesting properties [28,29], such as excellent thermal and acoustic insolation, low diffusivity of gases and liquids, high elasticity, low density and high porosity. In fact, the integration of cork for thermal protection in spacecraft and rockets began with the successful Apollo XI mission in 1969 [30]. The Poisson's ratio, taking the negative ratio of the strains normal and parallel to the in-plane loading directions in cork is rather low (0.25–0.5) [31,32], whereas the Poisson's ratio with loading along the prism axis is negligibly small (0–0.1). Dense rubber has a high Poisson's ratio (around 0.5), and in rubber elastomeric honeycombs the Poisson's ratio shows a full range of negative −1 up to 2 [31,33]. Due to these properties, cork has many applications beyond its massive use as wine stopper, e.g., in floors and walls owing thermal and acoustic insolation, but also in consumer goods (decoration, footwear, furnishing, bags), automotive and aerospace industries [34–36], just to mention a few. At present, the cork production world-wide exceeds 300.000 to 350.000 metric tons per

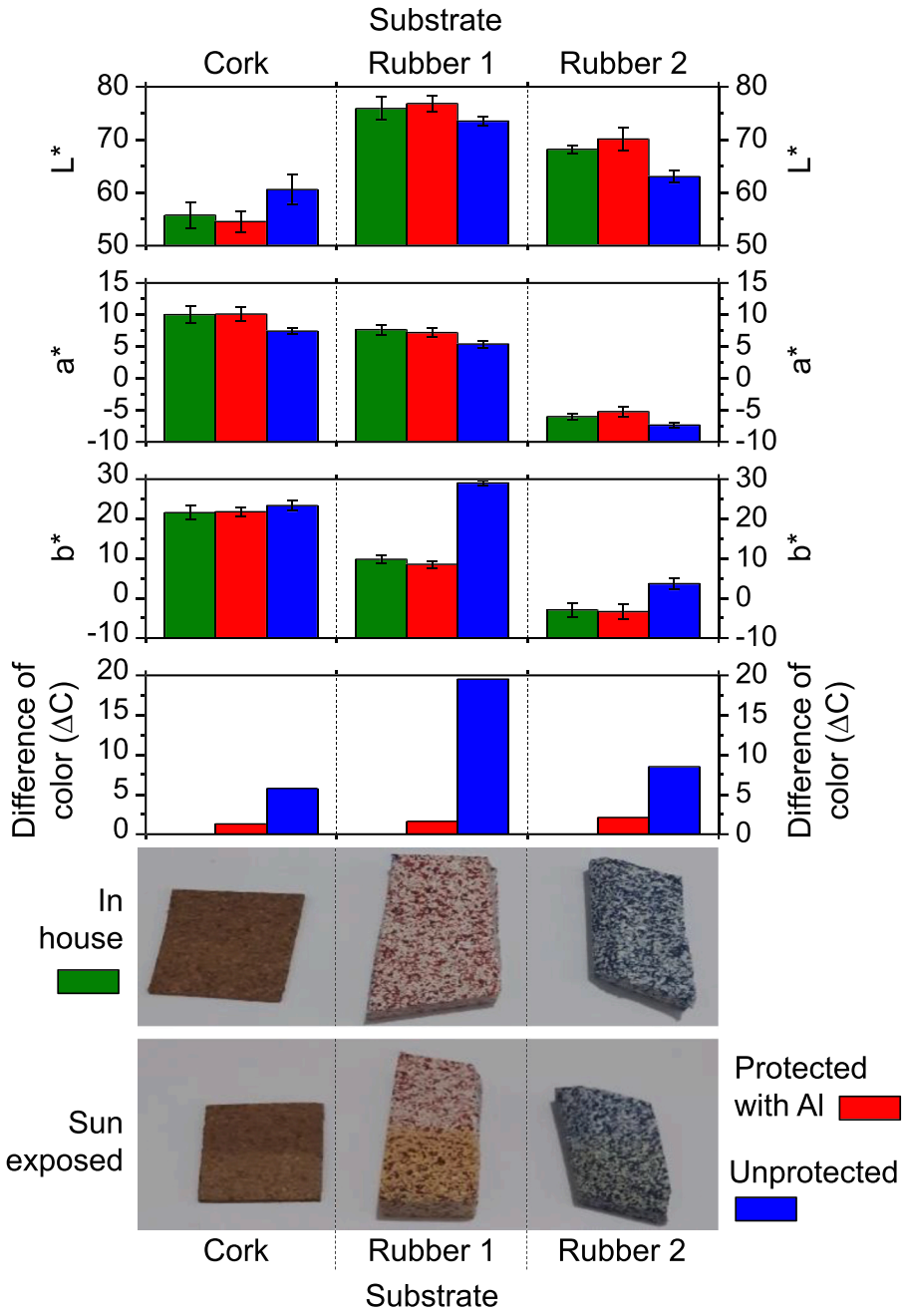

Fig. 6. Variation of color coordinates (L*, a* and b*) of cork and two rubbers with different binding resin after exposure of 10 days to sunlight protected and not protected with an Al foil. The overall color variation (ΔC, see Eq. (1)) with respect to the corresponding substrates kept in house is also depicted. Images of the three substrates in the three conditions are included in the bottom of the figure, i.e., in house, sun exposed and protected and sun exposed and unprotected.

year, being equivalent in volume to almost 20 million metric tons of steel [28,33]. Similar applications are found by composites of rubber particles embedded in resin [37,38].

However, when these materials are exposed to sunlight, their surface reveals rapidly ageing due to the UV radiation. The mechanisms of photo- and thermal ageing of elastomers are well-described in the literature [39,40], in which alkyl radicals and conjugate carbonyls are produced. However, the focus here does not lie on the radiative transfer processes as such, but on protection of elastomers against sunlight. Our approach is to protect these sensitive substrates (cork, as an example of a cellular elastomeric material, and rubber-resin composites) by the deposition of a UV-blocking protective film composed by an oxide transparent to visible sunlight, like TiO_2 [41]. Needless to say, cork being a cellular material represents an extremely challenging example in the category of 'complex substrates' for surface engineering; for instance, its microstructure is very inhomogeneous, with areas which are difficult to coat due to shadowing phenomena.

Fig. 6 shows the color coordinates (L*, a* and b*) of cork and two rubber composites with different resins under three exposures to sunlight: no exposure (kept indoors at dark), and two types of sun exposure during 10 days: protected with an aluminum foil and full exposure. The variation of color (ΔC, cf. Eq. (1)) with respect to the unexposed substrates is also included. Images of the three substrates under the three types of exposure are depicted at the bottom of Fig. 6. As expected, the color coordinates of the unexposed substrates (green bars) are similar to the substrate protected with aluminum foil (red bars), which lead to very low values of ΔC (Eq. (1)) for the three substrates ($\Delta C < 1$).

In contrast, a clear variation is observed when making a comparison with substrates exposed to sunlight but without protection (blue bars). For instance, it is observed that the lightness coordinate L* increases for cork, but it decreases for both rubbers. This agrees with the images displayed at the bottom of Fig. 6, where it is shown that cork becomes lighter whereas rubber becomes darker. In terms of chromatic coordinates (a* and b*), a decrease of a* (less red) and an increase of b* (more yellow) is observed for all the substrates; the latest is the main contribution of the color change in both rubbers, in agreement with what is depicted at the bottom images of Fig. 6. The variation of color (ΔC) of substrates exposed to sunlight is large. Among the three substrates, cork seems to be the most resistant, and the role of the resin is probably behind the differences observed between Rubber 1 and Rubber 2. This was the reason to perform additional experiments only with Rubber 2. During exposure to the sun, the samples reached temperatures above 40 °C, during part of the day. This fact might also have influence in the color changes, and it will be investigated posteriorly.

Fig. 7 shows cross-sectioned SEM images of TiO_2 films deposited on cork, rubber, and Si substrates. The thickness of the film deposited by magnetron sputtering varies between 144 nm for Si (Fig. 7c) and 181 nm for cork (Fig. 7a). The films are continuous, without any presence of cracks, and the growth seems to be dense and not columnar. Fig. 7d shows a cross-section image of a cork particle coated by ALD. In this case, the identification of the film is not possible due to the low thickness of the film and the complex microstructure of the cork (cf. the honeycomb structure). Nevertheless, Energy Dispersive Spectra (EDS) of the external and internal regions of the particles (red and blue rectangles, respectively) have been acquired, cf. Fig. 7e. Therefore, only C and O peaks can be detected in the inner part of the particle, while Ti, Cl, and a more intense peak of O are identified in the external region. These elements indicate the presence of a TiO_2 film, and residues of the ALD precursor. To our knowledge, this is the first report in literature of a deposition by PVD and CVD on cork.

Fig. 8 shows the color coordinates of cork and Rubber 2 sheets coated by magnetron sputtering under different sun exposures. It is worth mentioning that the variation of color (ΔC) is calculated with respect to the respective uncoated not-sun exposed substrates. First, a color variation is observed due to the deposition of the TiO_2 film in both substrates (green bars). The variation is slightly smaller than those caused by sun exposure to uncoated substrates (cf. Fig. 6), but they lie in a similar range. Sun exposure causes an additional variation of color, reaching

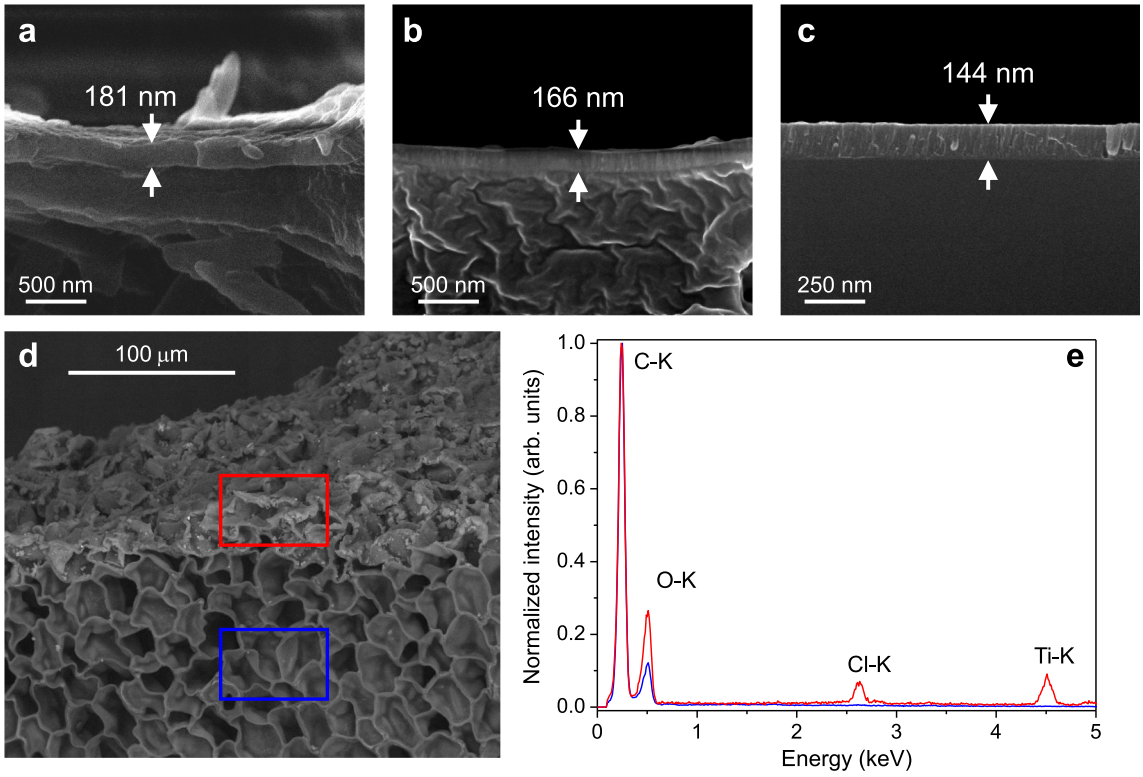

Fig. 7. Cross-section SEM images of TiO_2 films, deposited by magnetron sputtering on cork (a), rubber with resin (b) and silicon (c), and by ALD on a cork particle (d). The EDS spectra of the coated and uncoated areas of the particle, indicated by red and blue rectangles, respectively, are depicted on (e).

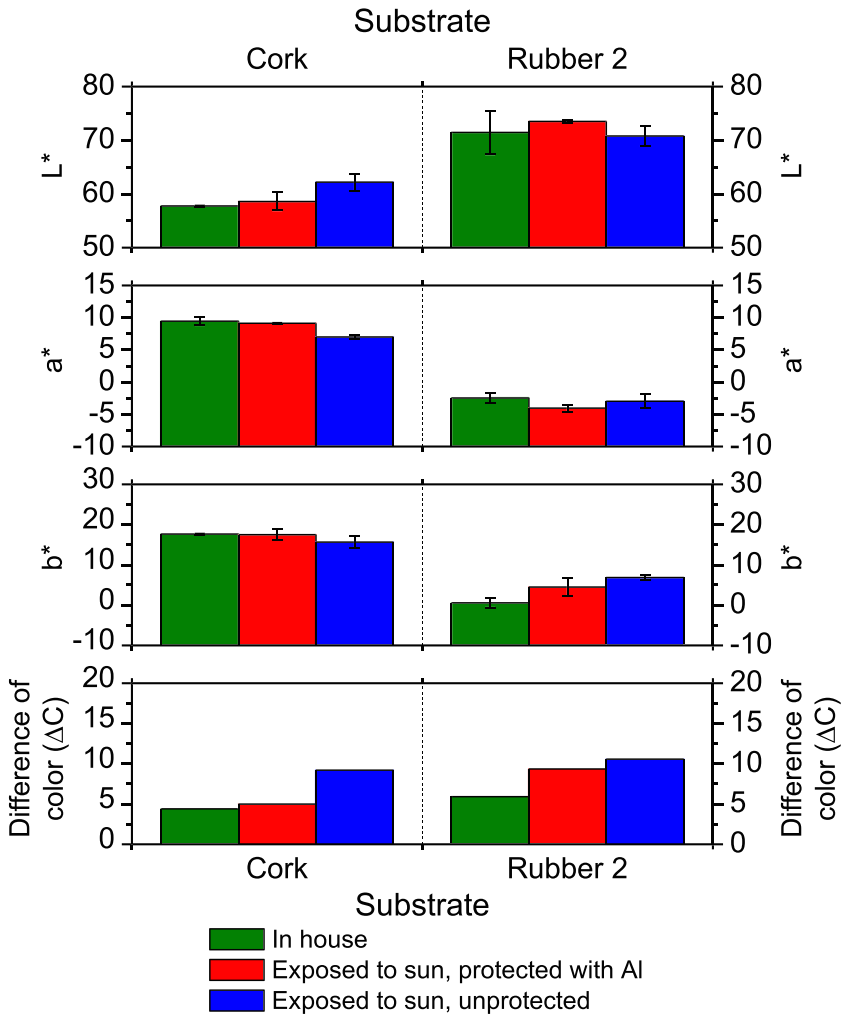

Fig. 8. Variation of color coordinates (L*, a* and b*) of cork and rubber substrates coated with TiO_2 after exposure of 10 days to sunlight protected and not protected with an Al foil. The overall color variation (ΔC, see Eq. (1)) with respect to the corresponding uncoated substrates kept in house (see Fig. 6) is also depicted.

overall ΔC values, which are larger than the corresponding ones for uncoated substrates. Nevertheless, a part of that variation is due to the deposition of the TiO_2 film.

The results obtained indicate that the deposited TiO_2 films failed to avoid the color variations of the substrates. First, the deposition of the film produces an unexpected color variation, which should be understood and avoided. Second, the substrates coated with TiO_2 films still suffer degradation under sunlight exposure. This may be attributed to rather poor UV-blocking properties of the TiO_2 films, which can be due to inappropriate crystallinity, structure, and/or phase composition. To discuss TiO_2 films on cork in a bit more detail and to position the results in the field of surface engineering we argue as follows.

In Section 1 it was stated that an almost bewildering choice of surface treatments covering a wide range of thickness has been developed in the past decades. Consequently, the feasibilities of protecting cork against UV have to be addressed in the first place. Indeed, from a crystallographic viewpoint, titania (TiO_2) is a very appealing coating material, i.e., with four crystalline forms at equilibrium (rutile, anatase, akaogiite and brookite) it has another 3 metastable and even another 5 high-pressure forms [42]. A common factor in the equilibrium structures is that Ti favors octahedral geometry, being bonded to six oxygen ions. The strongly lowered 4s band (due to ionicity) is responsible for inter-band absorption between 4s and 3d electronic band structure in the UV regime (around 3.5 eV and even higher in accordance with experiments and theoretical predictions), similar to all TiO complexes [43]. Indeed, intra-band transitions within 3d, e.g., $t_{2g}^* - e_g^*$, are also feasible but these transitions lie in the visible light spectrum (around, say 2.5 eV) [44], not in UV. Obviously, the refractive index in the visible light regime makes TiO_2 useful as optical antireflection coating and at the same time it can also be used as an inorganic UV absorber. For that reason, TiO_2 has been applied already for quite a while in sunscreen cosmetics, et cetera [45]. Therefore, TiO_2 is a good starting point as a UV light protecting coating, but combinations and even coatings onto TiO_2 with other oxides (SiO_2 and ZnO) may of course strengthen the UV absorbance.

As far as the deposition methodology of TiO_2 is concerned, besides magnetron sputtering and ALD reported here, wet chemical processes (i.e., of the sol-gel types) are quite suitable for the deposition of TiO_2 layers, also onto rough surfaces like cellular materials. The sols are produced starting from alkoxides as precursor; for instance, we have used a tetraethylorthotitanate precursor ($Ti(OC_2H_5)_4$, TEOTi) on flat substrates, not cellular, in the past [46]. This precursor results in a TiO_2 layer after deposition, gelation, and condensation. However, for getting a UV protecting coating, TiO_2 should be in a crystalline state (anatase but even better rutile), not in an (partly) amorphous state. In addition, the as-spun wet-chemical thin TiO_2 film has to be densified, and for that purpose a rather novel method to cure these TiO_2 layers at a higher rate was earlier designed based on laser technology [45,47].

Besides laser treatments, an alternative and more traditional post-treatment is of course curing in a tube furnace at higher temperatures.

Obviously, a furnace treatment will be at a much lower rate compared to the use of lasers. For metallic or ceramic substrates (steel, silica, alumina) these post-treatments at higher temperature are acceptable but definitely not for a cellular elastomer like cork. Please recall that the choice of the deposition method has to be such that the surface treatment does not impair too much the properties of the substrate for which it was originally chosen.

An escape route might be to apply a more recent nano-particle deposition method by fabricating with a high deposition rate TiO_2 nano-sized particles on polymer substrates at room temperature [48,49]. Some post-heat treatments might still necessary, which could represent a drawback in practical applications. Also, it is important to note that we proved through X-ray residual stress analysis [46] that large stresses (in the order of hundreds MPa) may evolve in the wet-chemical approach during processing. The residual stress is generated by the difference in thermal expansion coefficients with the substrate, and the temperature difference upon cooling from curing temperature to room temperature. Indeed, already during spinning and drying, tensile stresses usually evolve in TiO_2 due to capillary forces as a result of the evaporation of liquids in the solid network. However, these stresses are substantially reduced during the heating-up phase.

In comparison with sol-gel and other liquid-phase methods, magnetron sputtering has still a couple of advantages, i.e., higher deposition rate of TiO_2 and a better control of the film uniformity as well as morphology. Nevertheless, crystallinity is, like in the case of liquid-phase methods and nano-particle deposition methods, also here a major concern. At present the stress state is unknown.

Finally, it should be realized that TiO_2 may stimulate oxide photocatalysis through intra-d band transitions (see above, around 2.5 eV) in the visible light spectrum, as already observed after annealing in both doped [50] and undoped conditions [43]. This phenomenon may promote catalyzing reactions on the substrate leading to the degradation of the surface and variations of color. Therefore, an interesting idea is to explore the effect of additional interlayers (e.g., Al_2O_3) which will separate the substrate from the UV-blocking protective film.

As a result, our future research will be focused on a detailed analysis of the structural characteristics, together with the optical band gaps of these ALD/magnetron sputtered TiO_2 films on cork. Also, it has to be scrutinized whether a specific wavelength is responsible for the degradation process of the cork substrate, i.e., whether it is in the areas of absorption of the TiO_2 films. Other oxide coatings like ZnO and oxide composites will be investigated as well.

4. Conclusions

The use of thin films to improve a certain property of a substrate (e.g. protection) generally demands appropriate adhesion. However, the deposition of an adherent film on a complex substrate while avoiding the modification of its properties demands care and attention across the whole process. This work discusses three case studies of deposition of protective films on complex substrates.

For instance, cleaning of rubber was needed (restricted list of chemicals and conditions), and also surface activation with moderate biasing (avoiding high temperature variations) leads to positive contributions. In contrast, cleaning and surface activation in polished nylon has a detrimental effect on film adhesion. The complexity of the microstructure of the surface of the substrate has to be considered as well; in some cases (cork, rubber), polishing is not possible. In contrast, polishing was needed to remove the processing grooves of rigid Nylon, but it revealed an unexpected complicated internal structure, where the depth and finishing of polishing (and even the side of the piece) needed to be considered. It is worth mentioning that mechanical polishing has to be performed with care, even for more 'conventional' substrates such steel [51,52]. Deposition techniques with relatively lower directionality, such as ALD or bias-induced CVD, are interesting alternatives to coat substrates with complicated microstructure of the surface, since shadowing processes are reduced.

Other properties of this type of substrates allow interesting opportunities to improve the properties of the deposited films. In the case of rubber, the use of its large thermal expansion coefficient permitted us to tune the film microstructure through controlled cracking, and to improve the film flexibility without leaving any part of the surface unprotected. The polishing of nylon, once optimized, allowed us to deposit an adherent DLC film directly on the substrate, avoiding the deposition of interlayers or etching processes.

Ageing of cork and rubber-resin composites under sunlight was observed and a protective TiO_2 film was deposited by two different approaches: magnetron sputtering and atomic layer deposition. Although a complete substrate protection was still not achieved, to our knowledge, that is the first report in literature about deposition on a cellular elastomeric material, specifically cork.

Declaration of competing interest

The authors declare that they have no known competing financial interests or personal relationships that could have appeared to influence the work reported in this paper.

Acknowledgements

The authors congratulate Professor Allan Matthews with his 70th birthday and trust many fruitful and exciting years are still to come. The paper has been written in his honor as a tribute. We are eager to seize this opportunity to thank him for his stimulus provided over the years and for his international leadership in the field of processing-property relationships in surface engineering. Part of this research was carried out under project number MC7.06247 in the framework of the Research Program of the Materials innovation institute (M2i). Financial support of Portuguese Foundation of Science and Technology (FCT), under the projects IF/00671/2013, M-ERA-NET2/0012/2016, PTDC/CTM-REF/0155/2020, and Strategic Funding UIDB/04650/2020 is gratefully acknowledged.

References

[1] K. Holmberg, A. Erdemir, Influence of tribology on global energy consumption, costs and emissions, Friction 5 (2017) 263–284, https://doi.org/10.1007/s40544-017-0183-5.
[2] V. Bakolas, P. Roedel, O. Koch, M. Pausch, A first approximation of the global energy consumption of ball bearings, Tribol. Trans. 64 (2021) 883–890, https://doi.org/10.1080/10402004.2021.1946227.
[3] Claire Buysse, Joshua Miller, Sonsoles Díaz, Arijit Sen, Caleb Braun, The Role of the European Union's Vehicle CO2 Standards in Achieving the European Green Deal, International Council on Clean Transportation, 2021. https://theicct.org/wp-content/uploads/2021/06/EU-vehicle-standards-green-deal-mar21.pdf.
[4] P.M. Martin, Handbook of Deposition Technologies for Films and Coatings Science, Applications and Technology, Elsevier / WA, Amsterdam, Boston, 2010.
[5] B. Bhushan, Principles and Applications of Tribology, Second edition, Wiley, Chichester, West Sussex, UK, 2013.
[6] A. Leyland, A. Matthews, On the significance of the H/E ratio in wear control: a nanocomposite coating approach to optimised tribological behaviour, Wear. 246 (2000) 1–11, https://doi.org/10.1016/S0043-1648(00)00488-9.
[7] T.Y. Tsui, G.M. Pharr, W.C. Oliver, C.S. Bhatia, R.L. White, S. Anders, A. Anders, I. G. Brown, Nanoindentation and nanoscratching of hard carbon coatings for magnetic disks, MRS Proc. 383 (1995) 447, https://doi.org/10.1557/PROC-383-447.
[8] J. Musil, Hard and superhard nanocomposite coatings, Surf. Coat. Technol. 125 (2000) 322–330, https://doi.org/10.1016/S0257-8972(99)00586-1.
[9] J.F. Knott, Fundamentals of Fracture Mechanics, Butterworth, London, 1973.
[10] A. Matthews, A. Leyland, Developments in PVD tribological coatings, in: Proceedings of the 5th ASM Heat Treatment and Surface Engineering Conference in Europe, Gothenburg, Sweden, UK, 7–9 June 2000, ASM Int., Materials Park, OH, USA, 2000.
[11] A. Leyland, A. Matthews, Design criteria for wear-resistant nanostructured and glassy-metal coatings, Surf. Coat. Technol. 177–178 (2004) 317–324, https://doi.org/10.1016/j.surfcoat.2003.09.011.
[12] J.T.M. De Hosson, A. Cavaleiro, Galileo comes to the surface, in: Nanostructured Coatings, Springer, New York, 2006, pp. 1–27.
[13] F.P. Bowden, D. Tabor, The Friction and Lubrication of Solids, Clarendon Press; Oxford University Press, Oxford : New York, 2001.

[14] D. Martinez-Martinez, J.T.M. De Hosson, On the deposition and properties of DLC protective coatings on elastomers: a critical review, Surf. Coat. Technol. 258 (2014) 677–690, https://doi.org/10.1016/j.surfcoat.2014.08.016.
[15] G.A. Klein, Industrial Color Physics, 1st ed., Springer, London, 2010.
[16] J.P. van der Pal, D. Martinez-Martinez, Y.T. Pei, P. Rudolf, J.T.M. De Hosson, Microstructure and tribological performance of diamond-like carbon films deposited on hydrogenated rubber, Thin Solid Films 524 (2012) 218–223, https://doi.org/10.1016/j.tsf.2012.10.005.
[17] M. Schenkel, D. Martinez-Martinez, Y.T. Pei, J.T.M. De Hosson, Tribological performance of DLC films deposited on ACM rubber by PACVD, Surf. Coat. Technol. 205 (2011) 4838–4843, https://doi.org/10.1016/j.surfcoat.2011.04.072.
[18] D. Martinez-Martinez, M. Schenkel, Y.T. Pei, J.T.M. De Hosson, Microstructural and frictional control of diamond-like carbon films deposited on acrylic rubber by plasma assisted chemical vapor deposition, Thin Solid Films 519 (2011) 2213–2217, https://doi.org/10.1016/j.tsf.2010.11.006.
[19] B. Ollivier, S. Dowey, S. Young, A. Matthews, Adhesion assessment of dlc films on pet using a simple tensile tester - comparison of different theories, J. Adhes. Sci. Technol. 9 (1995) 769–784, https://doi.org/10.1163/156856195X00662.
[20] Y.T. Pei, D. Martinez-Martinez, J.P. van der Pal, X.L. Bui, X.B. Zhou, J.T.M. De Hosson, Flexible diamond-like carbon films on rubber: friction and the effect of viscoelastic deformation of rubber substrates, Acta Mater. 60 (2012) 7216–7225, https://doi.org/10.1016/j.actamat.2012.09.031.
[21] D. Martinez-Martinez, J.P. van der Pal, Y.T. Pei, J.T.M. De Hosson, Performance of diamond-like carbon-protected rubber under cyclic friction. I. Influence of substrate viscoelasticity on the depth evolution, J. Appl. Phys. 110 (2011), 124906, https://doi.org/10.1063/1.3665443.
[22] D. Martinez-Martinez, J.P. van der Pal, Y.T. Pei, J.T.M. De Hosson, Performance of diamond-like carbon-protected rubber under cyclic friction. II. Influence of substrate viscoelasticity on the friction evolution, J. Appl. Phys. 110 (2011), 124907, https://doi.org/10.1063/1.3665445.
[23] D. Martinez-Martinez, J.P. van der Pal, M. Schenkel, K.P. Shaha, Y.T. Pei, J.T.M. De Hosson, On the nature of the coefficient of friction of diamond-like carbon films deposited on rubber, J. Appl. Phys. 111 (2012), 114902, https://doi.org/10.1063/1.4723830.
[24] A. Niemczyk, D. Moszynski, A. Goszczynska, M. Kwiatkowska, A. Jedrzejczak, D. Nowak, J.G. Sosnicki, M. El Fray, J. Baranowska, Understanding the DLC film-polyamide 12 substrate interrelation during pulsed laser deposition, Appl. Surf. Sci. 576 (2022), https://doi.org/10.1016/j.apsusc.2021.151872.
[25] A. Igarashi, H. Hayashi, T. Yamanobe, T. Komoto, Structure and morphology of diamond-like carbon coated on nylon 66/poly(phenylene ether) alloy, J. Mol. Struct. 788 (2006) 238–245, https://doi.org/10.1016/j.molstruc.2005.12.005.
[26] W. Fruth, H. Meerkamm, T. Krumpiegl, C. Schaufler, G. Erkens, M. Ruttor, Tribological behaviour of PVD-coated PA plastic material sliding against metal counterparts, Surf. Coat. Technol. 120 (1999) 470–475, https://doi.org/10.1016/S0257-8972(99)00468-5.
[27] K. Baba, R. Hatada, Deposition of diamond-like carbon films on polymers by plasma source ion implantation, Thin Solid Films 506 (2006) 55–58, https://doi.org/10.1016/j.tsf.2005.08.072.
[28] H. Pereira, The rationale behind cork properties: a review of structure and chemistry, BioResources. 10 (2015) 6207–6229.
[29] S.P. Silva, M.A. Sabino, E.M. Fernandes, V.M. Correlo, L.F. Boesel, R.L. Reis, Cork: properties, capabilities and applications, Int. Mater. Rev. 50 (2005) 345–365, https://doi.org/10.1179/174328005X41168.
[30] James E. Pavlosky, Leslie G. St. Leger, Apollo Experience Report - Thermal Protection Subsystem, National Aeronautics and Space Administration, Lyndon B. Johnson Space Center, Houston, Texas, 1974. https://ntrs.nasa.gov/api/citations/19740007423/downloads/19740007423.pdf.
[31] M.A. Fortes, M. Teresa Nogueira, The poison effect in cork, Mater. Sci. Eng. A 122 (1989) 227–232, https://doi.org/10.1016/0921-5093(89)90634-5.
[32] L.J. Gibson, K.E. Easterling, M.F. Ashby, The structure and mechanics of cork, Proc. R. Soc. A. 377 (1981) 99–117.
[33] L.J. Gibson, M.F. Ashby, Cellular Solids, Cambridge Un. press, Cambridge, UK, 1997.
[34] M.M. Mateus, J.M. Bordado, R.G. dos Santos, Ultimate use of cork – unorthodox and innovative applications, Ciênc. Tecnol. Mater. 29 (2017) 65–72, https://doi.org/10.1016/j.ctmat.2016.03.005.
[35] M. Demertzi, A. Garrido, A.C. Dias, L. Arroja, Environmental performance of a cork floating floor, Mater. Des. 82 (2015) 317–325, https://doi.org/10.1016/j.matdes.2014.12.055.
[36] C. Ihamouchen, H. Djidjelli, A. Boukerrou, Development and characterization of a new cork-based material, Mater. Today Proc. 36 (2021) 34–40, https://doi.org/10.1016/j.matpr.2020.05.092.
[37] R.C. Popescu, D. Popescu, A.M. Grumezescu, Applications of rubber-based blends, in: Recent Dev. Polym. Macro Micro Nano Blends, Elsevier, 2017, pp. 75–109, https://doi.org/10.1016/B978-0-08-100408-1.00004-2.
[38] B. Chandra Ray, R. Kumar Prusty, D. Kumar Rathore, Fibrous Polymetric Composites, CRC Press, Taylor & Francis group, Boca Raton, FL, USA, 2018.
[39] L. Guo, G. Huang, J. Zheng, G. Li, Thermal oxidative degradation of styrene-butadiene rubber (SBR) studied by 2D correlation analysis and kinetic analysis, J. Therm. Anal. Calorim. 115 (2014) 647–657, https://doi.org/10.1007/s10973-013-3348-0.
[40] M.D. Romero-Sánchez, M. Mercedes Pastor-Blas, J.M. Martín-Martínez, M. J. Walzak, Addition of ozone in the UV radiation treatment of a synthetic styrene-butadiene-styrene (SBS) rubber, Int. J. Adhes. Adhes. 25 (2005) 358–370, https://doi.org/10.1016/j.ijadhadh.2004.12.001.
[41] C.-H. Wei, C.-M. Chang, Polycrystalline TiO2 thin films with different thicknesses deposited on unheated substrates using RF magnetron sputtering, Mater. Trans. 52 (2011) 554–559, https://doi.org/10.2320/matertrans.M2010358.
[42] H. Zhang, J.F. Banfield, Structural characteristics and mechanical and thermodynamic properties of nanocrystalline TiO 2, Chem. Rev. 114 (2014) 9613–9644, https://doi.org/10.1021/cr500072j.
[43] E. Vogelzang, J. Sjollema, H.J. Boer, J.T.M. De Hosson, Optical absorption in TiNxOy-compounds, J. Appl. Phys. 61 (1987) 4606–4611, https://doi.org/10.1063/1.338370.
[44] B. Liu, X. Zhao, Q. Zhao, X. He, J. Feng, Effect of heat treatment on the UV–vis–NIR and PL spectra of TiO2 films, J. Electron Spectrosc. Relat. Phenom. 148 (2005) 158–163, https://doi.org/10.1016/j.elspec.2005.05.003.
[45] A. Jaroenworaluck, W. Sunsaneeyametha, N. Kosachan, R. Stevens, Characteristics of silica-coated TiO2 and its UV absorption for sunscreen cosmetic applications, Surf. Interface Anal. 38 (2006) 473–477, https://doi.org/10.1002/sia.2313.
[46] J.T.M. de Hosson, D.H.J. Teeuw, Nanoceramic caotings produced by laser treatment, Surf. Eng. 15 (1999) 235–241, https://doi.org/10.1179/026708499101516588.
[47] D.H.J. Teeuw, M. de Haas, J.T.M. De Hosson, Residual stress fields in sol-gel-derived thin TiO2 layers, J. Mater. Res. 14 (1999) 1896–1903, https://doi.org/10.1557/JMR.1999.0254.
[48] D.-M. Chun, M.-H. Kim, J.-C. Lee, S.-H. Ahn, A Nano-particle deposition system for ceramic and metal coating at room temperature and low vacuum conditions, Int. J. Precis. Eng. Manuf. 9 (2008) 51–53.
[49] D.M. Chun, M.H. Kim, J.C. Lee, S.H. Ahn, TiO2 coating on metal and polymer substrates by nano-particle deposition system (NPDS), CIRP Ann. 57 (2008) 551–554, https://doi.org/10.1016/j.cirp.2008.03.111.
[50] R. Asahi, T. Morikawa, T. Ohwaki, K. Aoki, Y. Taga, Visible-light photocatalysis in nitrogen-doped titanium oxides, Science 293 (2001) 269–271, https://doi.org/10.1126/science.1061051.
[51] A.C. de Oliveira, M.C.L. de Oliveira, C.T. Ríos, R.A. Antunes, The effect of mechanical polishing and finishing on the corrosion resistance of AISI 304 stainless steel, Corros. Eng. Sci. Technol. 51 (2016) 416–428, https://doi.org/10.1080/1478422X.2015.1131493.
[52] K. Jaffré, B. Ter-Ovanessian, H. Abe, N. Mary, B. Normand, Y. Watanabe, Effect of mechanical surface treatments on the surface state and passive behavior of 304L stainless steel, Metals 11 (2021) 135, https://doi.org/10.3390/met11010135.